An applied theoretical framework to determine the suitability of ratiometric, two-state biosensors to measure biochemical properties in live animals

By Julian A. Stanley

An undergraduate honors interdisciplinary thesis submitted to

The Faculty of

the College of Science of

Northeastern University

as partial fulfillment for the requirements

for the degree of Bachelor of Science

April 19th, 2019

Thesis directed by

Javier M. Apfeld

Assistant Professor of Biology

Abstract of Thesis

Genetically-encoded biosensors have revolutionized our ability to measure a wide variety of cellular properties in live animals. As experimentalists, any time a new sensor is developed, we would like to know: what is that sensor good for? That is, what range of values of the cellular property of interest is that sensor well-suited to measure accurately? Here, we present a theoretical framework to determine the suitability of biosensors with two states.

Two-state biosensors are simple sensors that change conformation, and spectral properties, in response to a specific input. Existing two-state biosensors respond to a wide variety of important cellular properties, including pH, ATP, and glutathione redox potential. In our previous work with the roGFP1_R12 sensor, we deployed a mathematical framework that enabled us to calculate glutathione redox potential from fluorescence ratio measurements given knowledge of the spectral and biochemical properties of the sensor, and the properties of our microscope.

We extended this framework to analyze how the precision of microscopy measurements limits the accuracy of calculated glutathione redox potentials. This enabled us to predict the range of redox potentials that roGFP1_R12 is well-suited to measure given a theoretical measurement error and, importantly, with our empirically-determined measurement error. This analysis demonstrated that our sensor is well-suited to measure cytosolic glutathione redox potential in the feeding muscles of live *C. elegans* over a wide range of environmental and genetic conditions.

Next, we applied our theoretical framework to 10 glutathione redox potential sensors with known spectral and biochemical properties. This enabled us to define the range of potentials for which each sensor is well-suited and choose optimal sensors for different applications. Finally, we generalized our framework to all ratiometric two-state biosensors and applied this analysis to families of pH biosensors. To increase the accessibility of our framework, we have also begun to build web-based, interactive tools and documentation to help the community find biosensors that are well-suited for their experiments.

Table of Contents

List of Abbreviations and Constants

GFP	green fluorescent protein
redox	reduction-oxidization
roGFP	redox-sensitive green fluorescent protein
OxD	degree of oxidization (fraction oxidized)
GSH	glutathione
E_{GSH}	reduction-oxidization potential of glutathione
R	fluorescence ratio measurement
R_{min}	minimum possible fluorescence ratio measurement
R_{max}	maximum possible fluorescence ratio measurement
δ	dynamic range
δ_{λ_2}	relative allocation of the dynamic range in the second of two wavelengths
mV	millivolts
E°	midpoint potential
R_{gas}	ideal gas constant
T	temperature, in Kelvin
F	Faraday constant

List of Figures

1. Thesis background and preliminary analysis

Fluorescent protein biosensors

Biosensors are usually genetically-encoded proteins that emit fluorescence. A well-known one-state sensor is the wild-type green fluorescent protein (GFP). If you shine light at GFP, it enters an excited state where it fluoresces and emits light around $510\ nm$. The relative amount of light that GFP emits depends on the wavelength of light that initially excited the sensor (Figure 1.1). GFP is used for a wide variety of research purposes, such as visualizing the localization of cellular proteins.

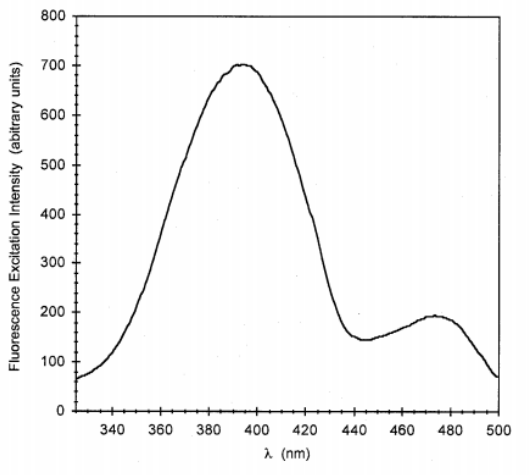

Figure 1.1: The emission spectra of wild-type GFP when emitted light is captured at 510 nm. Image from Mark Cannon's 2005 Thesis (personal correspondence).

Two-state fluorescent biosensors

Chemists have modified GFP to be sensitive to properties such as pH and glutathione redox potential. Many of these modified GFPs exist in one of two states. For example, redox-sensitive GFPs (roGFPs) are proteins that can exist in either an oxidized or a reduced state [1-3]. Since each state has a unique fluorescence excitation pattern, knowledge of (1) the

concentration of sensors and (2) the level of fluorescence emission at a certain wavelength can be used to determine the proportion of sensors in each state (Figure 1.2).

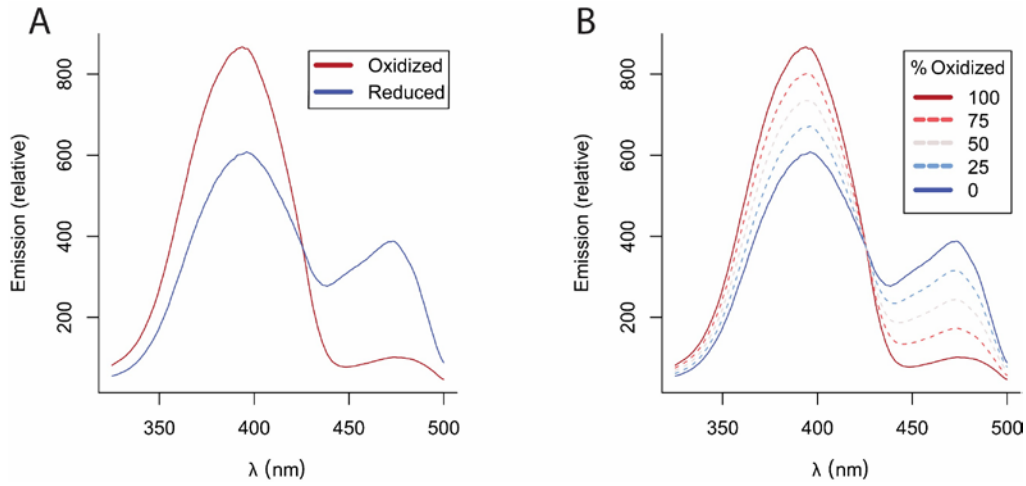

Figure 1.2: The emission spectra of the redox sensor roGFP1-R12. **(A)** Emission spectra of oxidized and reduced forms of a single sensor. **(B)** Weighted spectra of a population of sensors along with the corresponding proportion of oxidized sensors.

Intensity measurements from simple fluorescent microscopy can be used to determine the fraction of redox sensors that are oxidized, but those measurements also depend on sensor concentration, which is typically unknown. To obtain a concentration-independent indication of the fraction of sensors in each state, we use a ratio image from two different excitation wavelengths. From the ratio image we can create a unique map between fluorescence emission and redox potential. We have previously used ratiometric microscopy in *Caenorhabditis elegans*, which have revealed novel insights into the intercellular organization of redox potential [4]. Other groups have used roGFP sensors in bacteria, yeast, plants, mice, and human cell lines [5-12].

The ratio of sensor emission intensity (I) taken at two wavelengths (λ_1 and λ_2) is called R:

$$R = \frac{I_{\lambda_1}}{I_{\lambda_2}}$$

R is related to the proportion of sensors in an oxidized or reduced state. At the minimum ratio value (R_{min}), all sensors are reduced. As sensors become oxidized, the emission in the first wavelength (I_{λ_1}) increases and the emission in the second wavelength (I_{λ_2}) decreases. When the ratio emission reaches its maximum value (R_{max}), all sensors are oxidized. Previous groups have created functions that map between observed ratiometric measurement (R) and the fraction of oxidized sensor molecules (OxD), which is used as an input to the Nernst equation to determine the cellular glutathione redox potential (E_{GSH}) (Figure 1.3, Supplementary Material 1) [13, 14].

Spectra-defined parameters define the map between ratio and redox measurements

When we measure our sensor at a ratio of $R = \frac{I_{410}}{I_{470}}$, we can map between ratio and the fraction of oxidized sensors with (Figure 1.3B):

$$OxD = \frac{R - R_{min}}{\mathrm{R} - R_{min} + \delta_{470}(R_{max} - \mathrm{R})}$$

And between ratio and the glutathione redox potential with (Figure 1.3C):

$$E_{GSH} = E_{roGFP} = E^{\circ}_{roGFP} - \frac{R_{gas}T}{2F}\ln\left(\delta_{470} * \frac{R_{max} - R}{R - R_{min}}\right)$$

Where R_{gas} is the universal gas constant, T is the temperature in Kelvin, F is the Faraday constant, and E°_{roGFP} is the empirically-determined midpoint potential of the sensor ([13], See Supplementary Note 1 for full derivation).

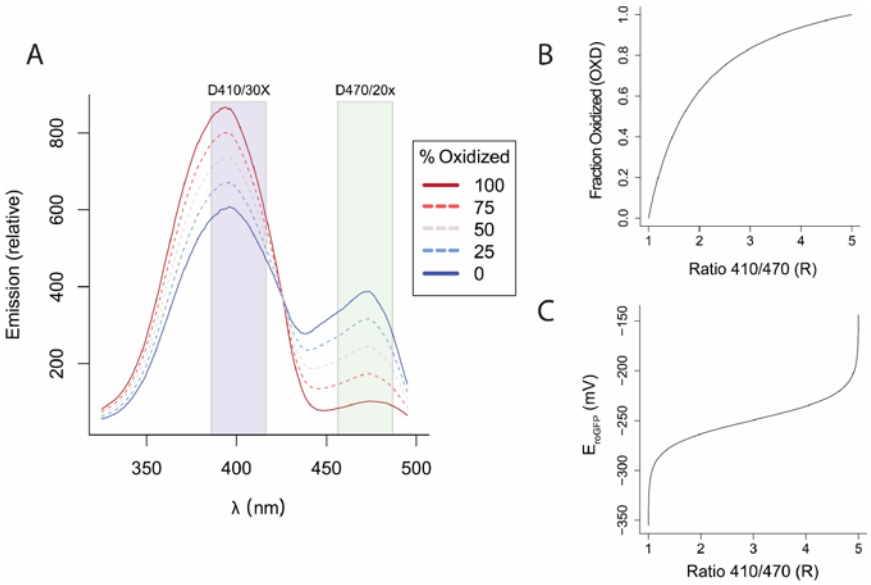

Figure 1.3:. The ratiometric properties of roGFP1-R12 and their maps to redox measurements. **(A)** The fluorescence emission spectra of roGFP1-R12. Ratiometric measurements can be made by exciting with light passed through filters such as D410/30X and D470/20X, shown as translucent rectangles. As the percentage of oxidized sensors changes, so does the distribution of emission around the isosbestic point (the point where the oxidized and reduced spectra overlap). **(B)** The map between ratio measurement and fraction oxidized, described by the equation $\mathrm{OxD} = \frac{\mathrm{R}-\mathrm{R_{min}}}{(\mathrm{R}-\mathrm{R_{min}})-\delta_{\lambda_2}(\mathrm{R}-\mathrm{R_{max}})}$ where R is the ratiometric measurement, $\mathrm{R_{min}}$ is the ratio when fully reduced, $\mathrm{R_{max}}$ is the ratio when fully oxidized, and δ_{λ_2} is the relative contribution of the second wavelength (in this case, $470\ \mathrm{nm}$) to the dynamic range. **(C)** The map between ratio measurement and redox potential, described by the equation $\mathrm{E_{GSH}} = \mathrm{E^{\circ}_{roGFP}} - \frac{\mathrm{R_{gas}T}}{2\mathrm{F}}\ln(\frac{1-\mathrm{OxD}}{\mathrm{OxD}})$ where E is the redox potential, $\mathrm{E^{\circ}}$ is the midpoint potential, $\mathrm{R_{gas}}$ is the gas constant, T is the temperature in Kelvin, and F is the Faraday constant.

Three constants define the maps between R and OxD and E_{GSH}: the maximum possible ratio value, R_{max}, the minimum possible ratio value, R_{min}, and a parameter we call δ_{λ_2}. A sensor's

dynamic range ($\frac{R_{max}}{R_{min}}$) is the ratio of the dynamic ranges of the sensor at two different excitation wavelengths. We call the dynamic range of the second wavelength δ_{λ_2}; in other words, $\frac{R_{max}}{R_{min}} = \frac{\delta_{\lambda_1}}{\delta_{\lambda_2}}$. Each of the three required constants—R_{min}, R_{max}, and δ_{λ_2}—can be calculated from the physical spectra of the sensor, if it is known. R_{min} can be calculated as the $\frac{410}{470}$ intensity ratio in the reduced state, R_{max} as the $\frac{410}{470}$ intensity ratio in the oxidized state, and δ_{470} as the ratio between oxidized and reduced intensity at $470\ nm$, $\frac{I_{470,Oxidized}}{I_{470,Reduced}}$ (Figure 1.4). These constants may also be defined empirically by maximally oxidizing and reducing the sensor [4].

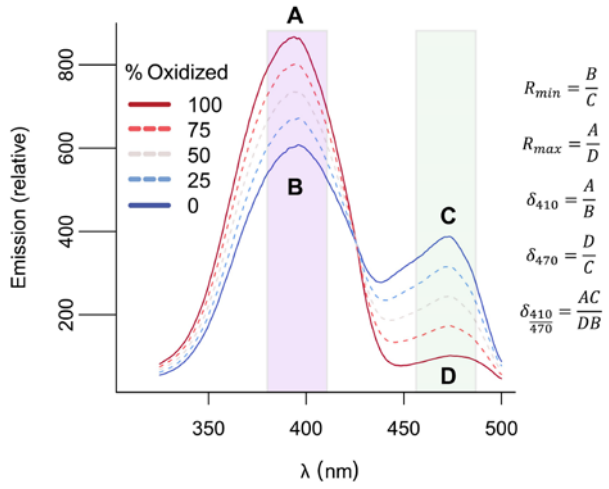

Figure 1.4: The emission intensity spectra for a population of roGFP1_R12 sensors with annotated features. Shown with band wavelengths of (purple) the D410/30X microscope filter and (green) the D470/20x filter. A, B, C, and D are labeled at $\mathrm{I}_{410,\mathrm{Oxidized}}$ $\mathrm{I}_{410,\mathrm{Reduced}}$, $\mathrm{I}_{470,\mathrm{Oxidized}}$, and $\mathrm{I}_{470,\mathrm{Reduced}}$, respectively. $\mathrm{R}_{\mathrm{min}}$ and $\mathrm{R}_{\mathrm{max}}$ are calculated as the $\frac{\mathrm{I}_{410}}{\mathrm{I}_{470}}$ ratios in the reduced and oxidized states, respectively. The δ_λ for any λ can be calculated as $\frac{\mathrm{I}_{\lambda,\mathrm{Oxidized}}}{\mathrm{I}_{\lambda,\mathrm{Reduced}}}$, and shown are the calculations for δ_{410}, δ_{470}, and $\delta_{\frac{410}{470}}$ as examples.

Given the R_{min}, R_{max}, and δ_{λ_2} values of a sensor, we can construct maps between ratio emission, the fraction oxidized (OxD), and the glutathione redox potential (E_{GSH}). Different

values of R_{min} and R_{max} change the upper and lower bounds, but not the shape, of these transformations.

The δ_{λ_2} value has different effects on the E_{GSH} and OxD maps. The δ_{λ_2} value affects the linearity of the OxD map. Larger and smaller $\log(\delta_\lambda)$ values produce a more concave up or concave down map, respectively. A δ_{λ_2} value of 1 produces a linear map between R and OxD (Figure 1.5A). The δ_{λ_2} value vertically shifts the E_{GSH} map.

We can define an adjusted midpoint potential, E°_{adj}, to account for the scaling due to δ_{λ_2}:

$$E_{GSH} = E^{\circ}_{roGFP} - \frac{R_{gas}T}{2F}\ln\left(\delta_{\lambda_2} * \frac{R_{max} - R}{R - R_{min}}\right)$$

$$\boldsymbol{E^{\circ}_{adj}} \equiv E^{\circ}_{roGFP} + \frac{R_{gas}T}{2F} ln(\delta_{\lambda_2})$$

$$E_{GSH} = \boldsymbol{E^{\circ}_{adj}} - \frac{R_{gas}T}{2F}\ln\left(\frac{R_{max} - R}{R - R_{min}}\right) \; and$$

Larger and smaller $\log(\delta_{\lambda_2})$ values shift the E_{GSH} map down and up, respectively. A map with a δ_{λ_2} value of 1 is centered at the midpoint potential (Figure 1.5B).

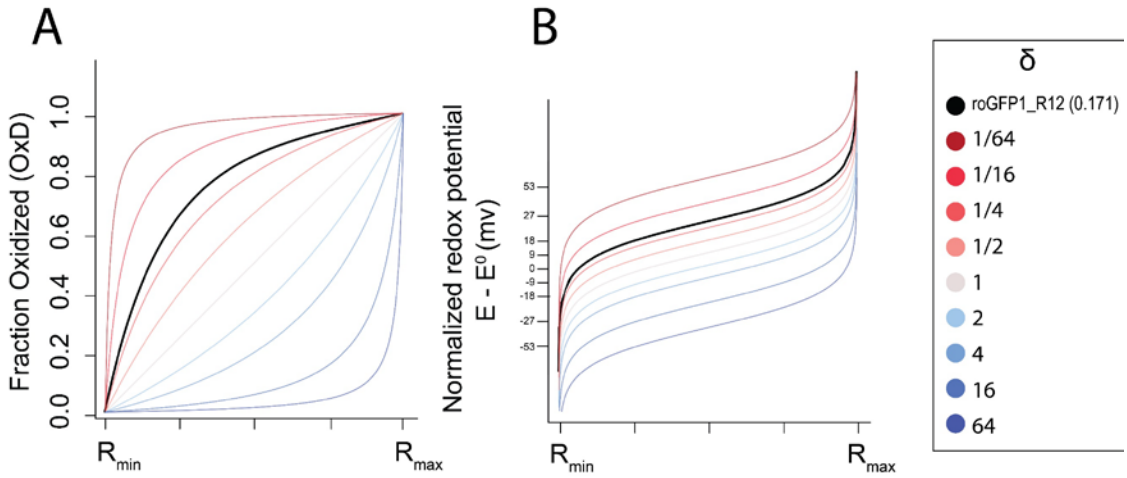

Figure 1.5: The map between ratio and fraction oxidized (OxD) and redox potential ($\mathrm{E_{GSH}}$). **(A)** The OxD map always ranges from $\mathrm{R_{min}}$ to $\mathrm{R_{max}}$ and the δ value determines the degree of linearity. roGFP1_R12 is concave down, since it has a δ_{470} of around 0.171. **(B)** The map between ratio and glutathione redox potential (E) always goes from $\mathrm{R_{min}}$ to $\mathrm{R_{max}}$ and the δ values determines the deviation of the apparent midpoint of the map from the true midpoint potential. roGFP1_R12 has an apparent midpoint potential that is approximately $22\ \mathrm{mV}$ higher than the true midpoint potential, since it has a δ_{470} of around 0.171.

Ratio-redox maps are affected by the choice of ratio wavelengths

The parameters that define the maps between R and OxD and E_{GSH} are themselves defined by the sensor's spectra (Figure 1.4). By changing the wavelengths at which you measure a sensor's ratio intensity, you can also change the maps.

To demonstrate the wavelength-dependences of the OxD and E_{GSH} maps, we examined how different choices of the second wavelength (λ_2 in $R = \frac{I_{\lambda_1}}{I_{\lambda_2}}$) in the ratio measurement would affect the maps. The value of δ_{λ_2} in the published spectrum of roGFP1_R12 varies widely across excitation wavelengths, from ~ 1.5 at $390\ nm$ to ~ 0.2 at $450\ nm$. Choosing values across the spectrum, the map between R and OxD ranged from concave up to concave down, and the map between R and E_{GSH} had adjusted midpoint potentials (E°_{adj}) ranging from $-270\ mV$ to $-244\ mV$ (Figure 1.6).

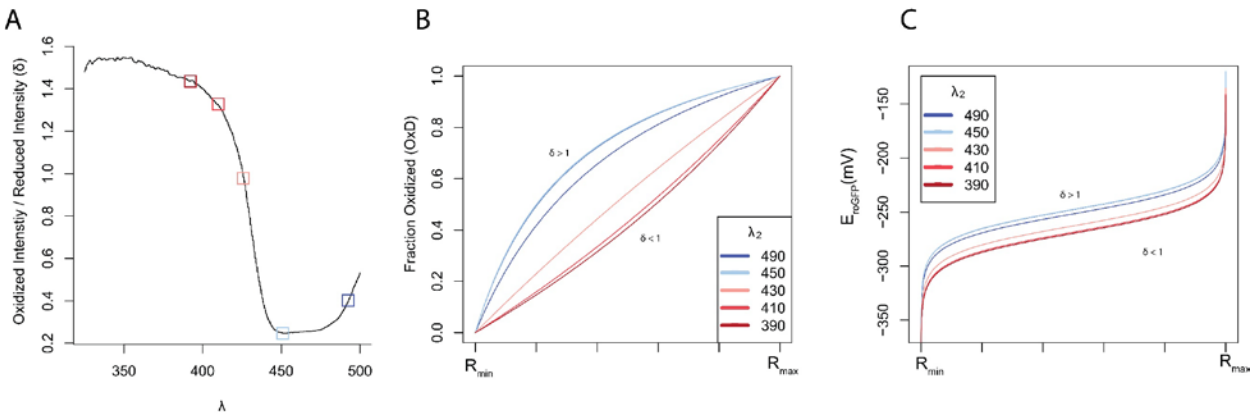

Figure 1.6: The choice of the second wavelength in the ratio image (λ_2) changes the map between ratio and biochemically-meaningful values in roGFP1_R12. **(A)** The value of δ_{λ_2} changes with the choice of second wavelength, with a fixed $\lambda_1 = 410\ nm$ **(B)** The linearity of the map between R and OxD changes based on the choice of second wavelength. **(C)** The map between R and $\mathrm{E_{GSH}}$ is linearly scaled based on the choice of second wavelength, with a fixed $\lambda_1 = 410\ nm$

2. Main thesis findings: sensitivity analysis

Empirical observations

We sought to examine how imprecision in microscopy measurements affect the estimates of the values of OxD and E_{GSH}. First, we determined the imprecision in our measurement of the ratio intensity, R. We found that the 95% confidence interval in our measurements was no larger than $(R_{True} * 0.97, R_{True} * 1.03)$, or a 3% relative error model described by $R_{Observed} = R_{True}(1 \pm 0.03)$ (Figure 2.1A).

With a 3% error in R, the error in OxD (ΔOxD) can be described as:

$$\Delta OxD = \left| \frac{[R(1 \pm 0.03)] - R_{min}}{[R(1 \pm 0.03)] - R_{min} + \delta_{470}(R_{max} - [R(1 \pm 0.03)])} - \frac{R - R_{min}}{\mathrm{R} - R_{min} + \delta_{470}(R_{max} - \mathrm{R})} \right|$$

And the error in glutathione redox potential (ΔE_{GSH}) as:

$$\Delta E_{GSH} = \left[-\frac{R_{gas}T}{2F} \ln\left(\delta_{470} \frac{R_{max} - [R(1 \pm 0.03)]}{[R(1 \pm 0.03)] - R_{min}} \right) \right] - \left[-\frac{R_{gas}T}{2F} \ln\left(\delta_{470} \frac{R_{max} - R}{R - R_{min}} \right) \right]$$

The propagated error into OxD relatively small. The error in E_{GSH} is also small near the map's center but explodes near the edges (Figure 2.1B, Figure 2.1C)

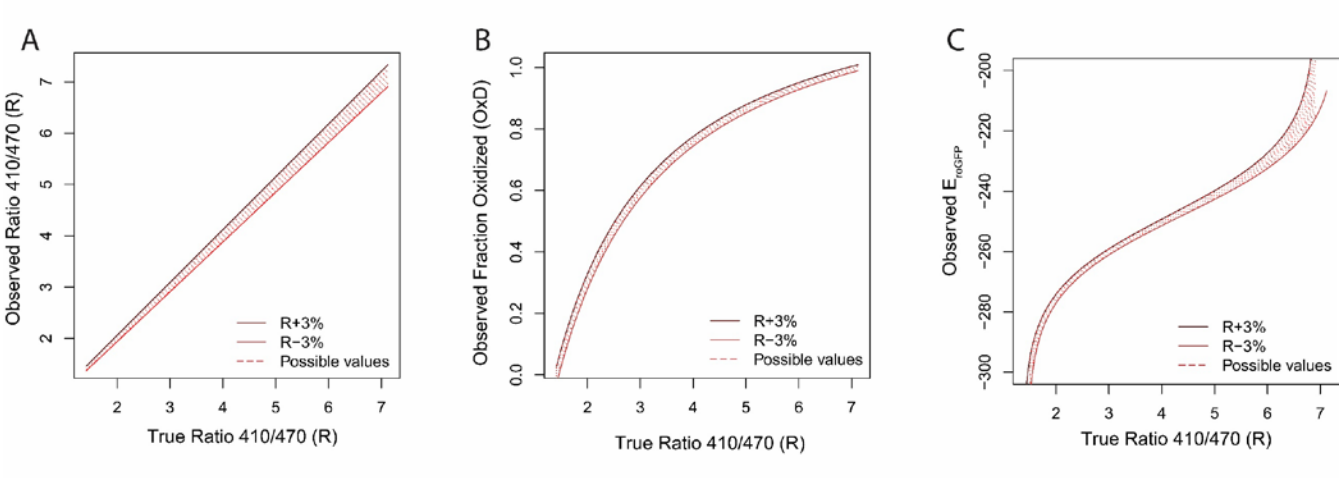

Figure 2.1: Propagation of microscopy error to redox error. **(A)** Our empirically-observed error model of $\mathrm{R_{Observed}} = \mathrm{R_{True}} * (1 \pm 0.03)$. **(B)** The effect of 3% microscopy error on the estimate of fraction oxidized (OxD). **(C)** The effect of 3% microscopy error on the estimate of glutathione redox potential $(\mathrm{E_{GSH}})$.

The relative sensitivity of the maps to a constant amount of error is given by the partial derivatives of those maps with respect to R. The sensitivity of E_{GSH} is only dependent on the R_{min} and R_{max}, while the sensitivity of OxD also depends on δ_{λ_2}. With a δ_{λ_2} greater than 1, measurements of OxD are most sensitive to imprecision in microscopy near R_{max}. With a δ_{λ_2} less than 1, those measurements are most sensitive near R_{min}. And, if the δ equals 1, OxD is equally sensitive to error across the entire dynamic range (Figure 2.2).

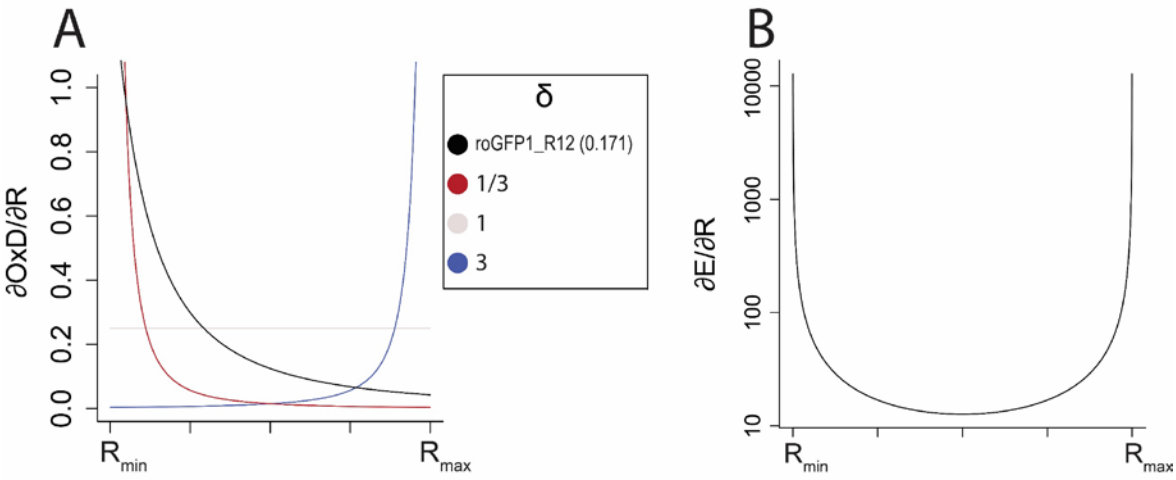

Figure 2.2: Sensitivities of redox values to microscopy error. **(A)** $\frac{\partial OxD}{\partial R}$, with different values of δ. Since δ changes the curvature of the $OxD(R)$ relationship, it also changes the derivative. **(B)** $\frac{\partial E}{\partial R}$, which is only dependent on the dynamic range.

Determining the effect of empirical precision on final measurements

We next sought to put our analysis into a more empirically-useful context. We noticed that all true ratio measurements map to some true glutathione redox potential. Using that observation, we modified the plot in Figure 2.1 to map between true redox potential values and the ranges of redox potentials one may observe 95% of the time (Figure 2.3A). Using this map, we can predict (1) the redox potentials that we are likely to observe when we measure some true redox potential as well as (2) a confidence interval of true redox potentials, given an observed redox potential. We then computed the error, or maximum deviation from truth, that one may observe at any given true redox potential (Figure 2.3B, Figure 2.3C).

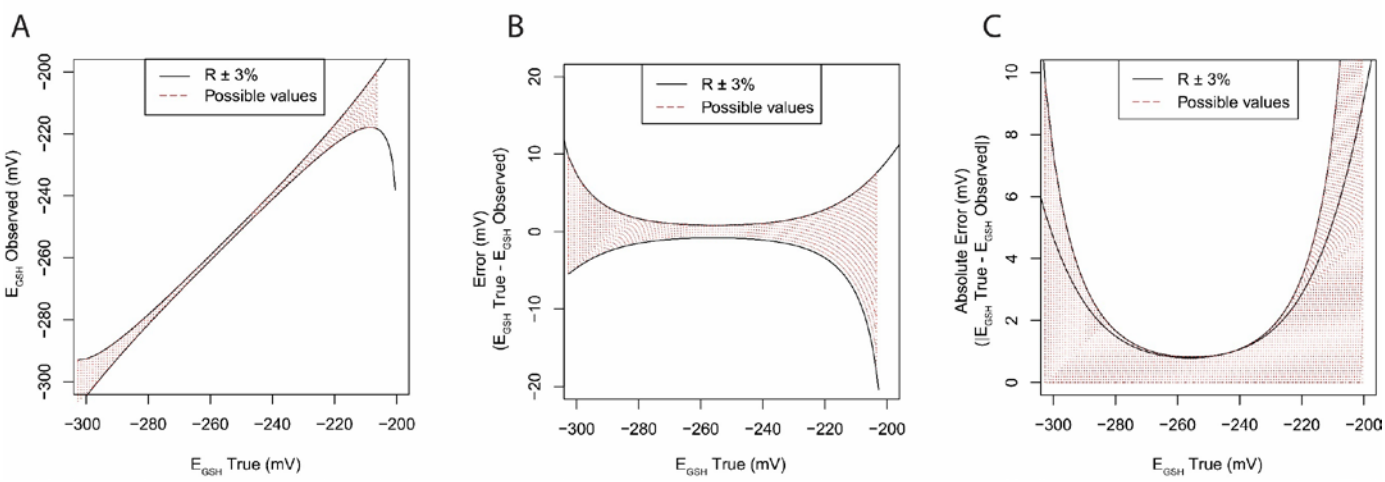

Figure 2.3: Possible errors in redox potential. **(A)** The map between true redox potentials ($E_{GSH}\ True$) and observed potentials ($E_{GSH}\ Observed$). **(B)** The map between true redox potentials ($E_{GSH}\ True$) and error ($E_{GSH}\ True - E_{GSH}\ Observed$) **(C)** The map between true redox potentials ($E_{GSH}\ True$) and absolute error ($|E_{GSH}\ True - E_{GSH}\ Observed|$).

At any true redox potential, there is some maximum amount of error that we could expect to see at that point, with 95% confidence (Figure 2.4A). By inverting the axes of that relationship, we can construct a phase plot. To use the phase plot, we first pick the maximum amount of inaccuracy we are willing to tolerate for an experiment. For example, we might want to measure redox potentials within $2\ mV$ of their actual values. Then, the cross sectional area of the phase curve represents the redox values that can be measured to that level of accuracy (Figure 2.4B).

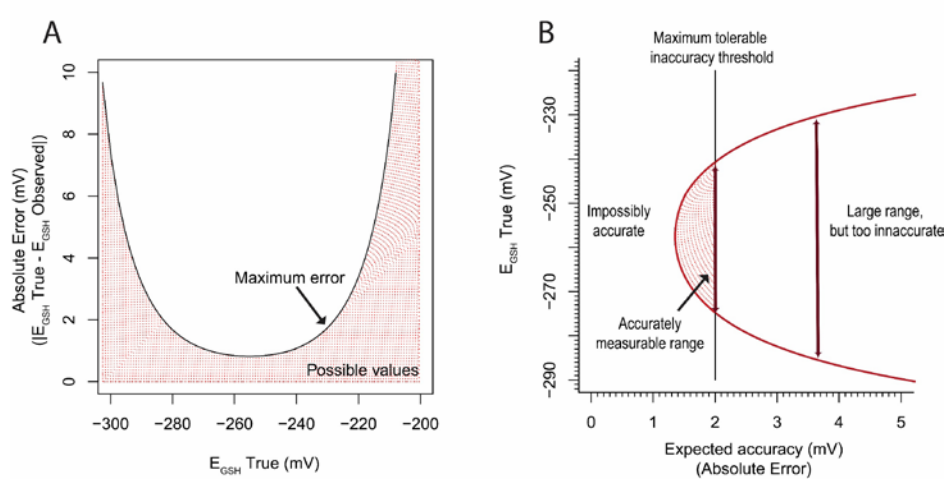

Figure 2.4: Defining the maximum expected accuracy at all redox potentials. **(A)** The maximum error observed (with 95% confidence) at any redox potential, assuming either 3% imprecision in microscopy. **(B)** By inverting panel 'A', we can construct a phase plot that describes the range of redox potentials one can reasonably expect to measure (vertical axis) to some pre-defined accuracy threshold (horizontal axis).

By taking a cross section of a phase curve from roGFP1_R12, we determined that the sensor is able measure individual redox potentials of -285 to -230 with an accuracy of at least $2\ mV$. Since redox potentials in the pharynx tend to fall between -280 and $-260\ mV$ [4], we conclude that, even with the imprecision in our microscope, the roGFP1_R12 sensor is well-suited to measure redox potentials in the *C. elegans* pharynx (Figure 2.5).

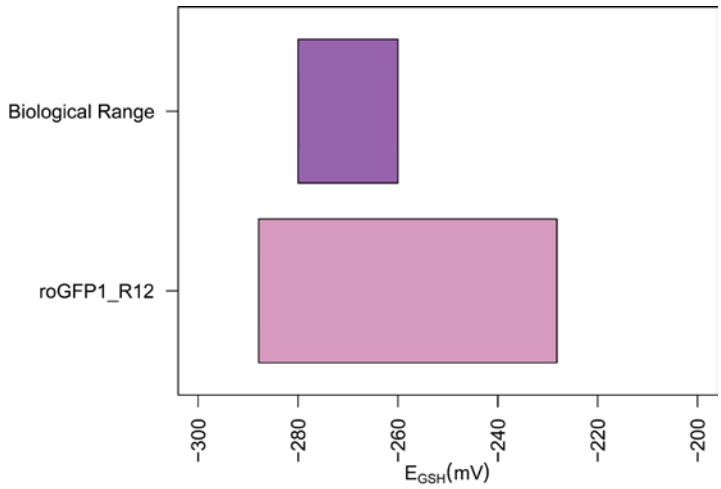

Figure 2.5: The range of redox potentials that roGFP1_R12 is suited to measure to a $2\ mV$ accuracy with our empirical microscopy imprecision, compared to the published biological range of the *C. elegans* pharynx.

Theoretical framework

A phase plot can be made for any redox sensor, as long as we know (1) the physical characteristics of the sensor, specifically R_{min}, R_{max}, δ_{λ_2}, and E°, and (2) the precision of the microscope, specifically an error model in the form of a function $R_{Observed} = f(R_{Expected})$. The physical characteristics of the sensor affect both the centering of the phase plot (the redox potential that can be measured with the highest accuracy) and its horizontal location (the minimum absolute error, or accuracy threshold). Microscope precision only affects the horizontal location of the phase plot (Figure 2.6).

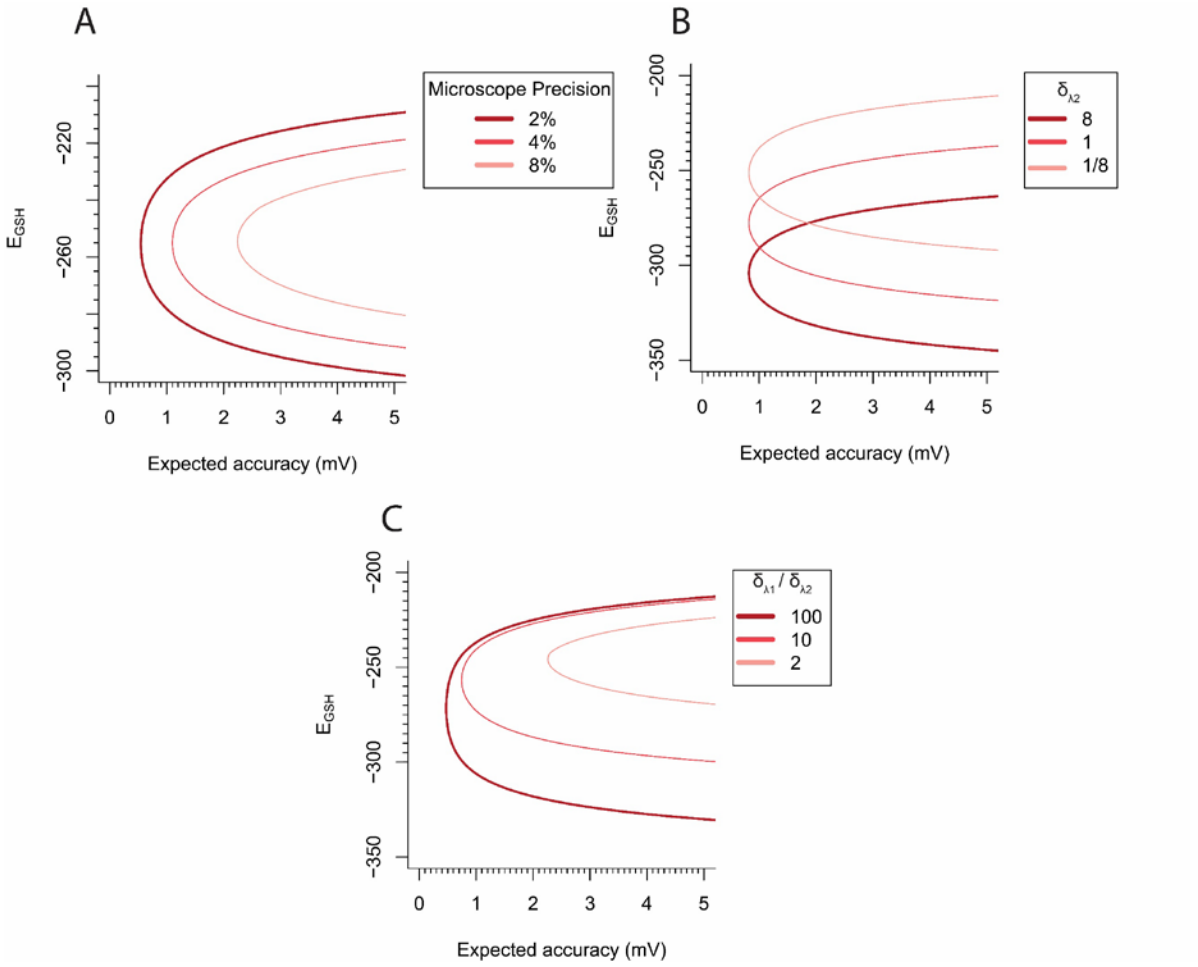

Figure 2.6: Phase plots for roGFP1_R12 with variable parameters. **(A)** With decreasing microscope precision, with errors from 2% to 8%. **(B)** With decreasing δ_{λ_2} values, from 8 to $1/8$, holding the dynamic range ($\frac{R_{min}}{R_{max}} = \frac{\delta_{\lambda_1}}{\delta_{\lambda_2}}$) constant **(C)** With decreasing dynamic ranges, holding δ_{λ_2} constant.

Applying of the framework to other redox sensors

We sought to ask what ranges of glutathione redox potentials we could measure if we had used a different biosensor. Using publicly-available spectra data, we computed the ranges that 10 roGFP-based sensors would be suitable to measure to a precision of $2\ mV$ (Supplementary Note 2). The ranges show a wide overlap between the redox potentials measured by roGFP1-

roGFP6, grx1_roGFP2, roGFP1_R12 and roGFP1_R9, which are each well-suited to measuring redox potentials in the cytosol. roGFP2_iL and roGFP1_iE were both designed to measurements in the endoplasmic reticulum (ER), and both appear to be well suited to measure in that environment, although the range of values measurable by roGFP2_iL appears much smaller than that measurable by roGFP1_iE (Figure 2.7).

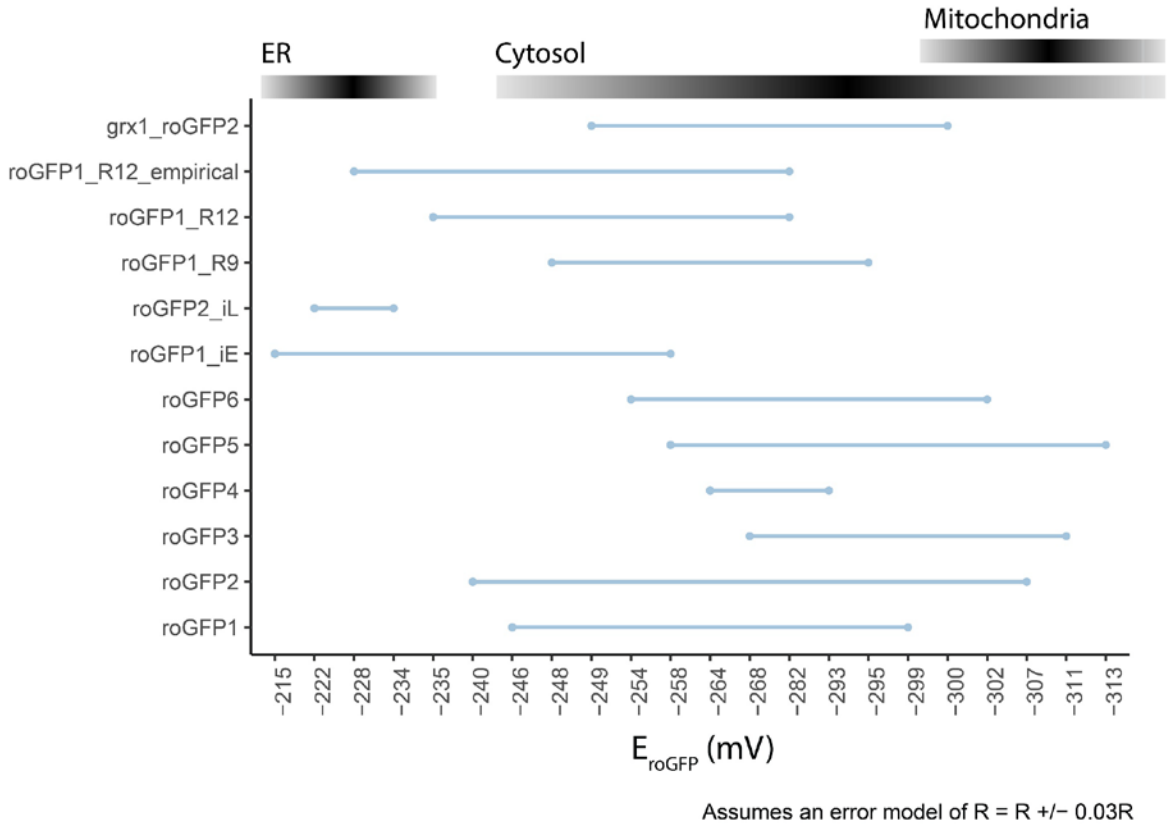

Figure 2.7: Suitable ranges for measurements with $2\ mV$ accuracy for published redox sensors. Top brackets represent estimates of the ranges of glutathione redox potentials in the endoplasmic reticulum (ER), cytosol, and mitochondria [15, 16]. The “roGFP1_R12_emprical” range is constructed from the parameters measured in the Apfeld lab, whereas the “roGFP1_R12” range is constructed from spectra obtained via personal correspondence with the Remington lab.

Generalizing the framework to any two-state, ratiometric sensor

The framework outlined for the roGFP sensors is applicable to any measurement taken with sensors that (1) have two states, and (2) are measured using ratiometric fluorescent microscopy.

At any time, such a sensor will be in either State-1 or State-2. The R_{max} of that sensor represents the ratio value when all the sensors are in State-1, and the R_{min} represents the ratio value when all the sensors are in State-2.

Just as we could describe the fraction of oxidized roGFP sensors, we can describe the fraction of sensors in State-1:

$$\frac{State_1}{State_1 + State_2} = \frac{R - R_{min}}{\mathrm{R} - R_{min} + \delta_{\lambda_2}(R_{max} - \mathrm{R})}$$

We can also similarly describe the error in that fraction, given some error in microscopy ϵ:

$$\Delta \frac{State_1}{State_1 + State_2} = \left| \frac{[R(1 \pm \epsilon)] - R_{min}}{[R(1 \pm \epsilon)] - R_{min} + \delta_{\lambda_2}(R_{max} - [R(1 \pm \epsilon)])} - \frac{R - R_{min}}{\mathrm{R} - R_{min} + \delta_{\lambda_2}(R_{max} - \mathrm{R})} \right|$$

Just as roGFP sensors use the fraction OxD to convert into redox potential, other sensors also have functions that map between the fraction of sensors in State-1 and some biologically-meaningful measurement. Using the same basic principles, we can construct a phase map for any two-state ratiometric sensor.

Applying the more general framework to pH sensors

Due to the similarity between redox potentials and pH, we sought to validate our model's generalizability using pH biosensors.

Two-state pH biosensors can be either protonated or deprotonated. When ratiometric emission measurements (R) are recorded from the sensors, the fraction of sensors in the deprotonated state ($FrDeprot = \frac{A^-}{A^- + HA}$) can be described as:

$$FrDeprot = \frac{A^-}{A^- + HA} = \frac{R - R_{min}}{\mathrm{R} - R_{min} + \delta_{\lambda_2}(R_{max} - \mathrm{R})}$$

The relationship between pH and the fraction in the deprotonated state can similarity be described based on the Henderson-Hasselbalch equation:

$$pH = pKa + \log\left(\frac{FrDeprot}{1 - FrDeprot}\right) = pKa + \log(\delta_{470}) + \log(\frac{R_{max} - R}{R - R_{min}})$$

We applied our model to four pH sensors with published emission spectra: deGFP1, deGFP4, pHRed, and mKemma [17, 18]. We mapped each true pH with the corresponding ranges of pH that could be observed, given our empirical microscopy error, and used that map to construct a phase plot (Supplementary Note 2). Based on the phase plot, we were able to map the ranges of pH that each of the four selected pH biosensors are well-suited to measure (Figure 2.8).

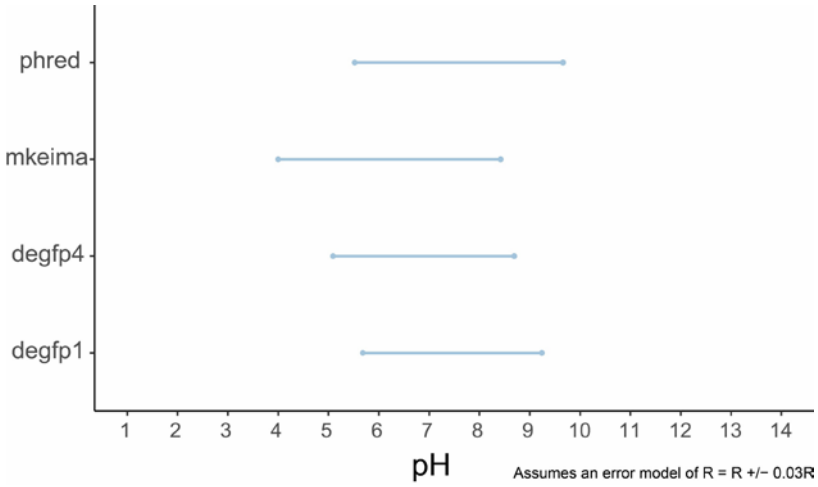

Figure 2.8: Suitable ranges for measurements with 0.1 pH-units accuracy for a subset of published pH sensors.

Conclusion

When designing an experiment to record a cellular property in living animals, it is crucial to choose a biosensor well-suited to the experimental question of interest. Currently, experimentalists may choose a biosensor based on physical properties, such as midpoint potential, that are only loosely associated with the ranges of values a sensor is well-suited to measure.

Here, we have presented a framework that allows for a more formal evaluation of a sensor, based on published spectral data. Using the framework, we can visualize the ability of a sensor to measure certain values to certain accuracies using an error phase plot. From the phase plot, we can extract the ranges of values a sensor is well-suited to measure at some level of accuracy. This more formal analysis can guide experimental design is two main ways. First, it is a realistic way to compare biosensors *in silico.* Different sensors are best suited to measure different ranges of values but, until now, no published framework explicitly defined those

ranges. Second, it allows for a critical analysis of errors within an experiment. For example, this framework could warn an experimentalist that measurement error is very high in the range of values they are measuring and that they should increase their sample sizes or attempt to increase the precision in their microscopy.

We are continuing to work to extend our framework to more two-state ratiometric sensors, such as ATP sensors, as well as consider how it may apply to more complicated, multistate sensors. We hope that our work will make it easier for microscopists to critically evaluate the errors in their experiments and choose a biosensor well-suited to their needs.

References

1. Cannon MB, Remington SJ: **Re-engineering redox-sensitive green fluorescent protein for improved response rate**. *Protein Sci* 2006, **15**(1):45-57.
2. Cannon MB, Remington SJ: **Redox-sensitive green fluorescent protein: probes for dynamic intracellular redox responses. A review**. *Methods Mol Biol* 2008, **476**:51-65.
3. Hanson GT, Aggeler R, Oglesbee D, Cannon M, Capaldi RA, Tsien RY, Remington SJ: **Investigating mitochondrial redox potential with redox-sensitive green fluorescent protein indicators**. *J Biol Chem* 2004, **279**(13):13044-13053.
4. Romero-Aristizabal C, Marks DS, Fontana W, Apfeld J: **Regulated spatial organization and sensitivity of cytosolic protein oxidation in Caenorhabditis elegans**. *Nat Commun* 2014, **5**:5020.
5. Fisher-Wellman KH, Neufer PD: **Linking mitochondrial bioenergetics to insulin resistance via redox biology**. *Trends Endocrinol Metab* 2012, **23**(3):142-153.
6. Hempel N, Ye H, Abessi B, Mian B, Melendez JAJFRB, Medicine: **Altered redox status accompanies progression to metastatic human bladder cancer**. 2009, **46**(1):42-50.
7. Wolf AM, Nishimaki K, Kamimura N, Ohta SJJoID: **Real-time monitoring of oxidative stress in live mouse skin**. 2014, **134**(6):1701-1709.
8. Higuchi R, Vevea JD, Swayne TC, Chojnowski R, Hill V, Boldogh IR, Pon LAJCB: **Actin dynamics affect mitochondrial quality control and aging in budding yeast**. 2013, **23**(23):2417-2422.
9. Sivakumar K, Mukherjee M, Cheng HI, Zhang Y, Ji L, Cao BJB, bioengineering: **Surface display of roGFP for monitoring redox status of extracellular microenvironments in Shewanella oneidensis biofilms**. 2015, **112**(3):512-520.
10. Rosenwasser S, Rot I, Meyer AJ, Feldman L, Jiang K, Friedman HJPP: **A fluorometer-based method for monitoring oxidation of redox-sensitive GFP (roGFP) during development and extended dark stress**. 2010, **138**(4):493-502.
11. Wagener KC, Kolbrink B, Dietrich K, Kizina KM, Terwitte LS, Kempkes B, Bao G, Müller MJA, signaling r: **Redox indicator mice stably expressing genetically encoded neuronal roGFP: versatile tools to decipher subcellular redox dynamics in neuropathophysiology**. 2016, **25**(1):41-58.
12. Jiang K, Schwarzer C, Lally E, Zhang S, Ruzin S, Machen T, Remington SJ, Feldman LJPp: **Expression and characterization of a redox-sensing green fluorescent protein (reduction-oxidation-sensitive green fluorescent protein) in Arabidopsis**. 2006, **141**(2):397-403.
13. Meyer AJ, Dick TP: **Fluorescent protein-based redox probes**. *Antioxid Redox Signal* 2010, **13**(5):621-650.
14. Delic M, Rebnegger C, Wanka F, Puxbaum V, Haberhauer-Troyer C, Hann S, Köllensperger G, Mattanovich D, Gasser BJFRB, Medicine: **Oxidative protein folding and unfolded protein response elicit differing redox regulation in endoplasmic reticulum and cytosol of yeast**. 2012, **52**(9):2000-2012.
15. Jones DP, Go Y-M: **Redox compartmentalization and cellular stress**. 2010, **12**(s2):116-125.

16. Markus S, P. DT, J. MA, Bruce M: **Dissecting Redox Biology Using Fluorescent Protein Sensors**. 2016, **24**(13):680-712.
17. Hanson GT, McAnaney TB, Park ES, Rendell ME, Yarbrough DK, Chu S, Xi L, Boxer SG, Montrose MH, Remington SJJB: **Green fluorescent protein variants as ratiometric dual emission pH sensors. 1. Structural characterization and preliminary application**. 2002, **41**(52):15477-15488.
18. Tantama M, Hung YP, Yellen GJJotACS: **Imaging intracellular pH in live cells with a genetically encoded red fluorescent protein sensor**. 2011, **133**(26):10034-10037.

3. Thesis reproducibility and dissemination: online tools

SensorOverlord R package

We have built a S4 class-based R package called SensorOverlord. The source code can be found at **https://github.com/julianstanley/SensorOverlord** and can be installed using the *install_github("julianstanley/sensorOverlord")* command from the *devtools* package in R.

In summary, the package takes (1) A biosensor spectra (in the form of a 4-column matrix) or the empirically-determined values for R_{min}, R_{max}, δ_{λ_2}, and the midpoint of the property of interest ($E°, pKa,$ etc), (2) a function describing the microscopy errors, and (3) the desired accuracy, and returns a phase plot and the ranges for which that sensor is well-suited to measure (Figure 3.1).

The package structure is built on the S4 object system in R. The package is centered behind a *Sensor* class, from which specific sensor classes, *redoxSensor* and *pHSensor* inherit. Any class that inherits from *Sensor* contains a *Rmin*, *Rmax*, and *delta*. *Sensor* objects can be initiated directly with these three fields or generated from a matrix of spectra values. More specific sensor objects can be initiated with (1) a *Sensor* object and (2) a class-specific midpoint (*e0* and *pKa* fields for *redoxSensor* and *pHSensor*, respectively).

Various generic methods are defined for the *Sensor* class, including ones that plot all of the figures in this thesis. Each of those methods are detailed to CRAN check standards in the package documentation.

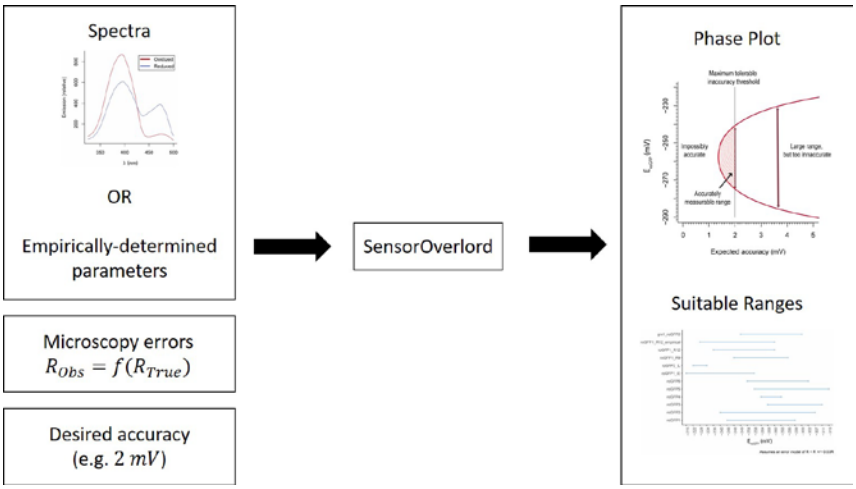

Figure 3.1: The general pipeline for analyzing two-state ratiometric biosensors. Spectra, empirical microscopy errors, and an accuracy threshold are given to the sensorOverlord framework, which produces phase plots and suitable ranges.

Publicly-hosted Jupyter notebook and web applications

We have created Jupyter notebooks that detail the steps to reproduce the sensitivity analysis presented in this thesis. Static versions of these notebooks can be found at **https://github.com/julianstanley/SensorOverlord_Notebooks** and full interactive versions of the notebooks are hosted at **https://mybinder.org/v2/gh/julianstanley/SensorOverlord_Notebooks/master.**

Further, we are currently developing interactive web applications to further increase the accessibility of the model to the broader public. One early web application allows users to input redox sensor parameters and interactively see how those parameters, as well as empirical microscopy precision, change the resulting errors in redox potential. That application is hosted at **https://julianstanley.shinyapps.io/Quick_SensorError/** and applications that allow more direct input of other sensor types are under development.

4. Supplementary material

Supplementary Note 1 — Derivations of ratio-redox maps

The intensity values emitted from the roGFP1-R12-containing tissue are recorded after being exposed to 410nm and 470nm light. The ratios between these emission values describe relative levels of tissue oxidation. For example, a 410/470 ratio of 2.0 indicates that a tissue is more oxidized than a ratio of 1.0. But how exactly does a ratio intensity value correspond to the proportion of oxidized tissues in a cell? Here we derive the equations for those maps.

Map from ratio intensity to degree of oxidation

Assume a fully reduced state. Then, the intensities observed at a wavelength λ are equal to the product of N_T, the total number of roGFP molecules, and $i_{\lambda,R}$, the intensity of each roGFP molecule at a given wavelength in the reduced state.

$$I_{\lambda,R} = N_T * i_{\lambda,R}$$

The same is true for the fully oxidized state:

$$I_{\lambda,X} = N_T * i_{\lambda,X}$$

At any redox state between maximally reduced and maximally oxidized, the intensity at a given wavelength is a weighted sum of the molecules found at either discretely oxidized or reduced state. We therefore can rewrite any observed intensity as the weighted sum of two states:

$$I_\lambda = \frac{N_X}{N_T} * I_{\lambda,X} + \frac{N_{Red}}{N_T} * I_{\lambda,R} \quad (1)$$

Because all sensor molecules must be in either an oxidized or reduced state, $N_R = N_T - N_X$.

So, we can rewrite equation (1) as a function of only the fraction in one state:

$$I_\lambda = \frac{N_X}{N_T} * I_{\lambda,X} + (1 - \frac{N_X}{N_T}) * I_{\lambda,R} \quad (2)$$

Using equation (2), consider the intensity ratio taken after excitation at $\frac{\lambda_1}{\lambda_2}$:

$$\frac{I_{\lambda_1}}{I_{\lambda_2}} = \frac{\frac{N_X}{N_T} * I_{\lambda_1,X} + (1 - \frac{N_X}{N_T}) * I_{\lambda_1,R}}{\frac{N_X}{N_T} * I_{\lambda_2,X} + (1 - \frac{N_X}{N_T}) * I_{\lambda_2,R}}$$

For brevity, let $OxD = \frac{N_X}{N_T}$. Then cross-multiply:

$$I_{\lambda_1} * OxD * (I_{\lambda_2,X} + (1 - OxD) * I_{\lambda_2,R}) =$$

$$I_{\lambda_2} * OxD * (I_{\lambda_1,X} + (1 - OxD) * I_{\lambda_1 R})$$

Simplify and express OxD in terms of known quantities:

$$OxD = \frac{I_{\lambda_2} I_{\lambda_1,R} - I_{\lambda_1} I_{\lambda_2,R}}{I_{\lambda_1} I_{\lambda_2,X} - I_{\lambda_1} I_{\lambda_2,R} - I_{\lambda_2} I_{\lambda_1 X} + I_{\lambda_2} I_{\lambda_1,R}}$$

To further simplify, let:

$$R_{Red} = \frac{I_{\lambda_1,R}}{I_{\lambda_2,R}} = R_{min}$$

$$R_X = \frac{I_{\lambda_1,X}}{I_{\lambda_2,X}} = R_{max}$$

$$R = \frac{I_{\lambda_1}}{I_{\lambda_2}}$$

$$\delta_{\lambda 2} = \frac{I_{\lambda_{1,X}}}{I_{\lambda_{2_R}}}$$

We can now re-derive the definition of OxD in terms of ratio values.

First, re-arrange terms and multiply by $\frac{-1}{-1}$:

$$OxD = \frac{I_{\lambda_1} I_{\lambda_2,R} - I_{\lambda_2} I_{\lambda_1,R}}{I_{\lambda_1} I_{\lambda_2,R} - I_{\lambda_2} I_{,\lambda_1 R} + I_{\lambda_2} I_{\lambda_1 X} - I_{\lambda_2 X} I_{\lambda_1}}$$

Then factor out $I_{\lambda_2,R} I_{\lambda_2}$ from the numerator and denominator write some in terms of ratio values:

$$OxD = \frac{I_{\lambda_2,R} I_{\lambda_2}(\mathrm{R} - R_R)}{I_{\lambda_2,R} I_{\lambda_2}(\mathrm{R} - R_R + \delta_{\lambda 2}(R_X - \mathrm{R}))}$$

And simplify:

$$OxD = \frac{R - R_{min}}{\mathrm{R} - R_{min} + \delta_{\lambda 2}(R_{max} - \mathrm{R})} \quad (3)$$

Where $\delta_{\lambda 2}$ describes the simple intensity dynamic range after excitation at λ_2.

Map from ratio intensity to redox potential

We can then describe the redox potential of the redox-sensitive sensor protein using the Nernst equation:

$$E_{roGFP} = E^{\circ}_{roGFP2} - \frac{RT}{2F}\ln\left(\frac{1 - OxD_{roGFP}}{OxD_{roGFP}}\right)$$

Where E°_{roGFP2} is the sensor's midpoint potential, R is the gas constant, T is the temperature in Kelvin, and F is the faraday constant.

If the sensor is in equilibrium with glutathione, the same equation also determines the redox potential of the glutathione couple:

$$E_{GSH} = E^{\circ}_{roGFP2} - \frac{RT}{2F}\ln\left(\frac{1 - OxD_{roGFP}}{OxD_{roGFP}}\right) \quad (4)$$

By plugging in the OxD equation (3), we can also express the glutathione redox potential as a function of R:

$$E_{GSH} = E^{\circ}_{roGFP2} - \frac{RT}{2F}\ln\left(\delta_{\lambda_2}\frac{R_{max} - R}{R - R_{min}}\right) \quad (4)$$

Supplementary Note 2 — Additional sensor information

Redox Sensors: Spectra

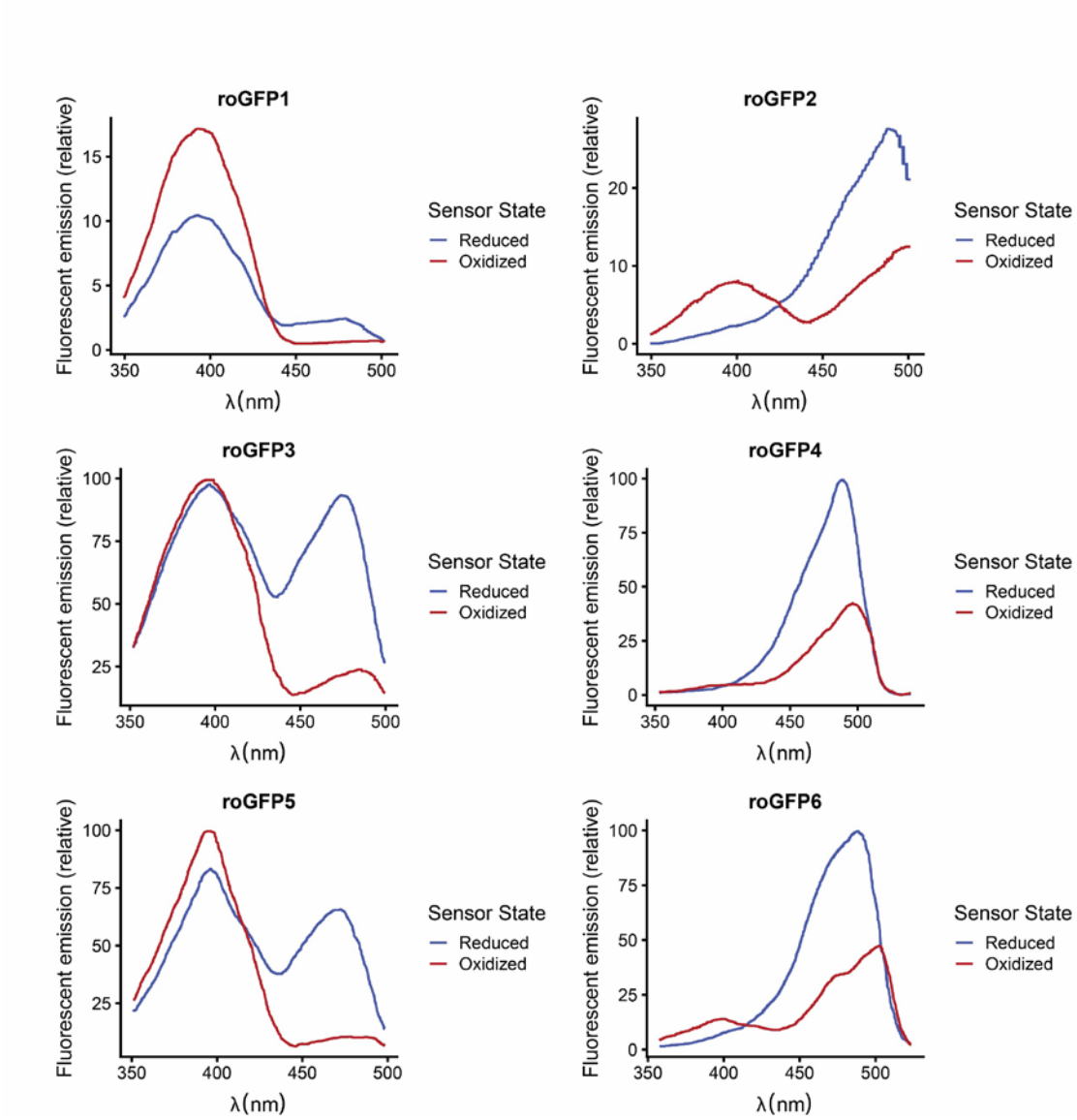

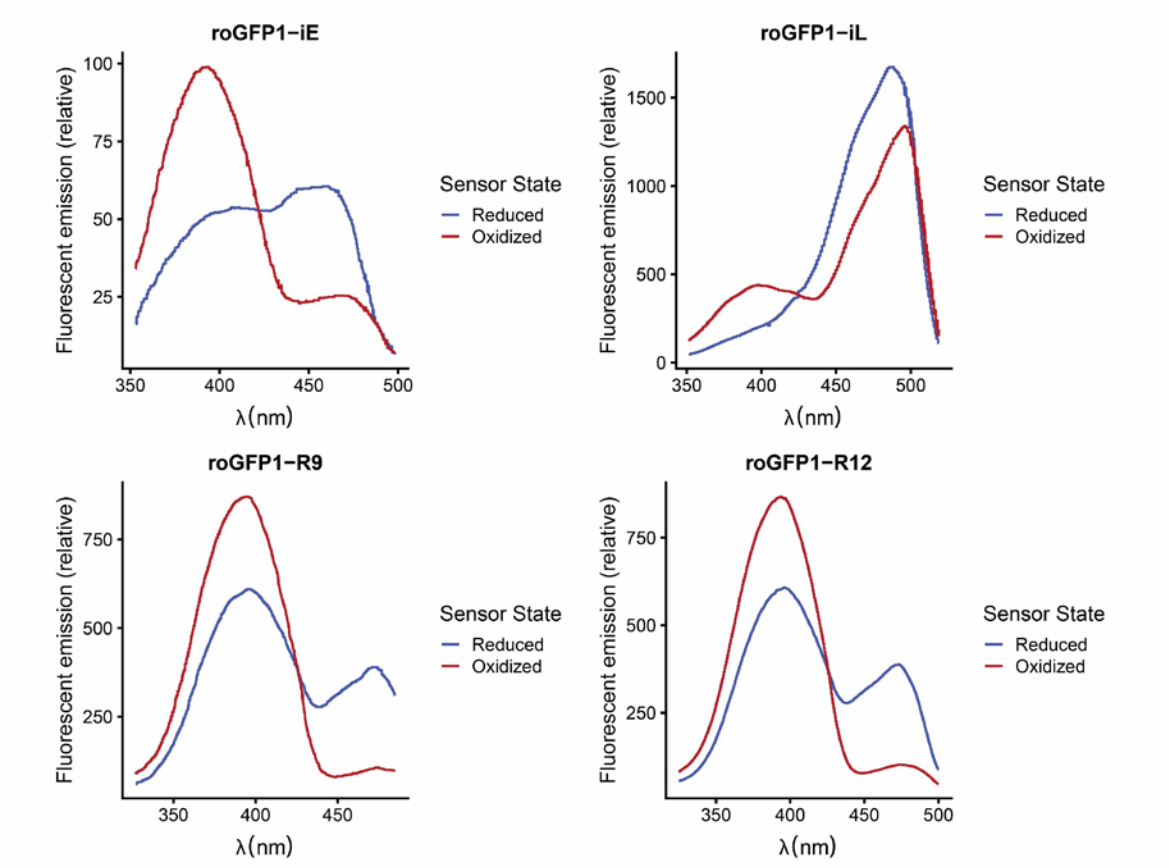
roGFP1−iE
roGFP1−iL
roGFP1−R9
roGFP1−R12
Fluorescent emission (relative)
λ(nm)
Sensor State
Reduced
Oxidized

Redox Sensors: Observed-actual maps and phase plots

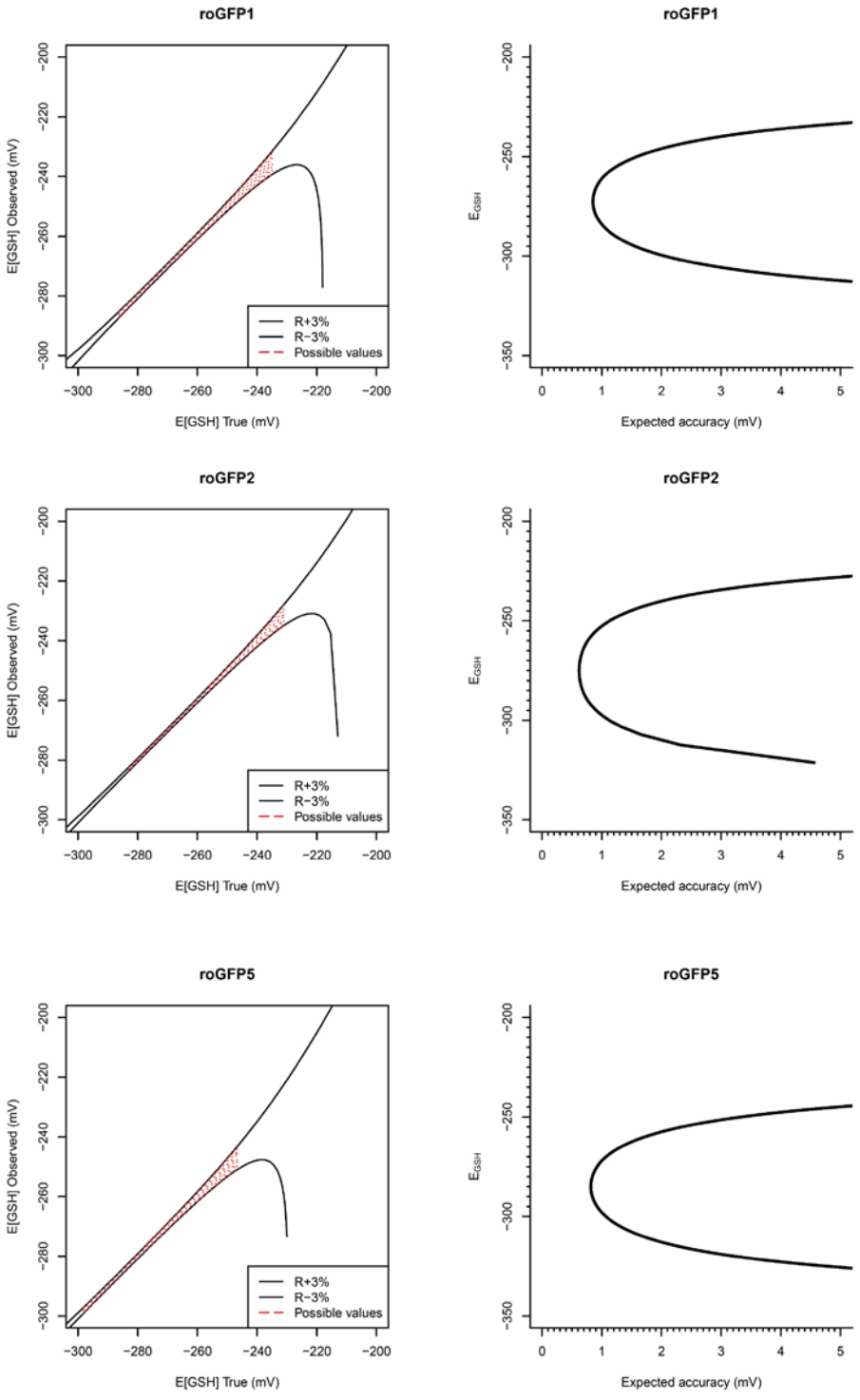

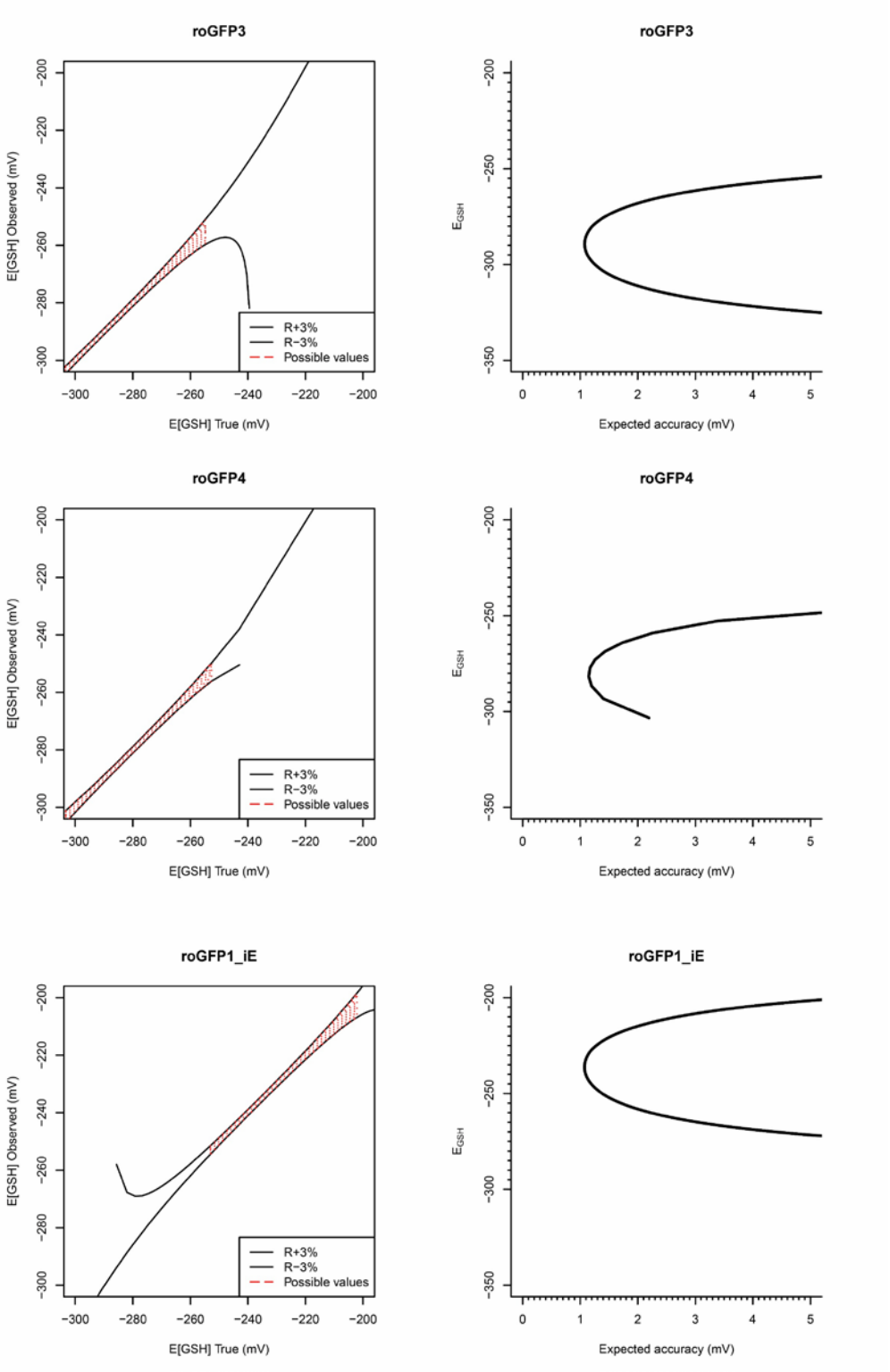
roGFP3
E[GSH] Observed (mV)
E[GSH] True (mV)
R+3%
R−3%
Possible values
roGFP3
E_{GSH}
Expected accuracy (mV)
roGFP4
E[GSH] Observed (mV)
E[GSH] True (mV)
R+3%
R−3%
Possible values
roGFP4
E_{GSH}
Expected accuracy (mV)
roGFP1_iE
E[GSH] Observed (mV)
E[GSH] True (mV)
R+3%
R−3%
Possible values
roGFP1_iE
E_{GSH}
Expected accuracy (mV)

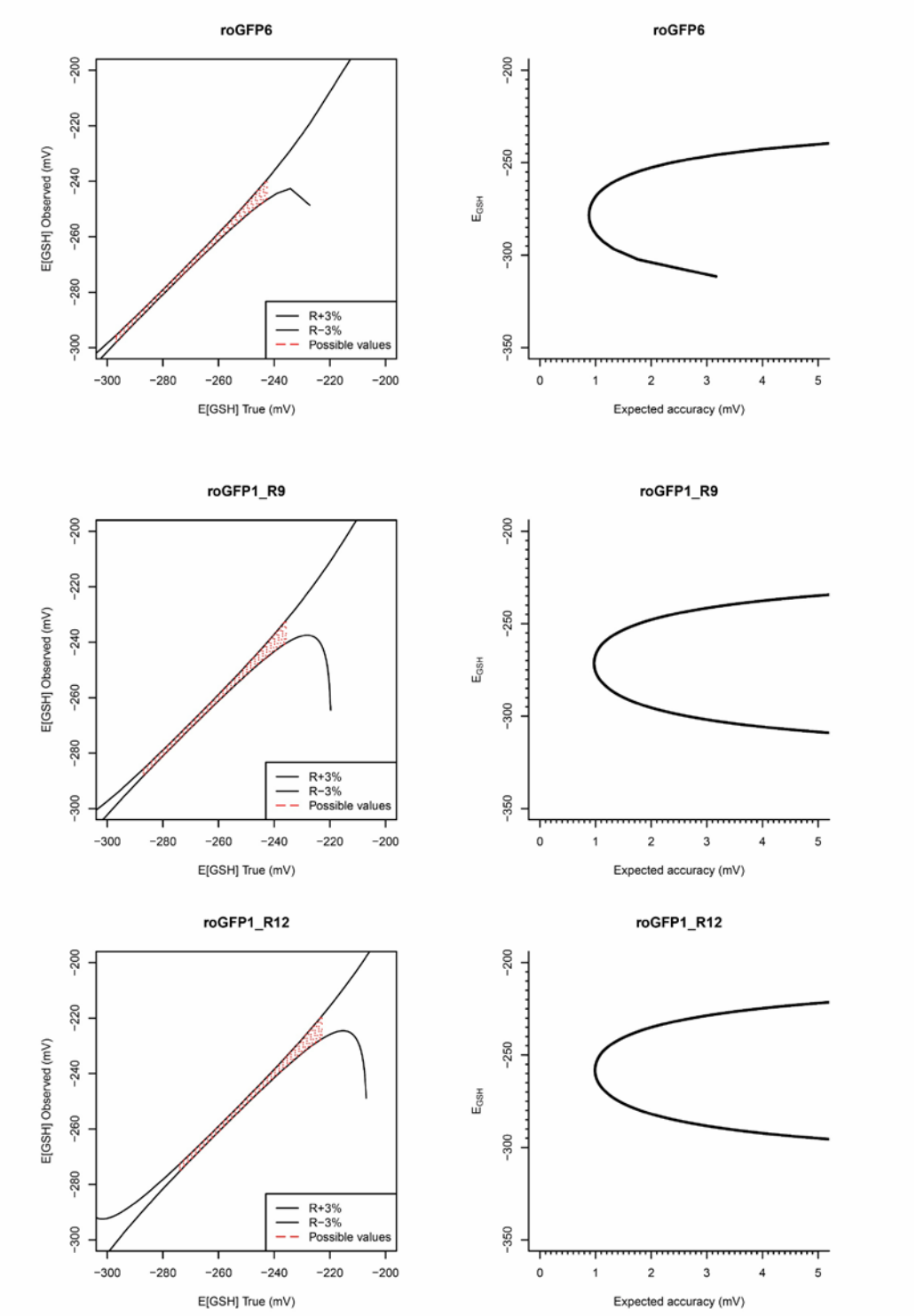
roGFP6
E[GSH] Observed (mV)
E[GSH] True (mV)
R+3%
R−3%
Possible values
roGFP6
E_{GSH}
Expected accuracy (mV)
roGFP1_R9
E[GSH] Observed (mV)
E[GSH] True (mV)
R+3%
R−3%
Possible values
roGFP1_R9
E_{GSH}
Expected accuracy (mV)
roGFP1_R12
E[GSH] Observed (mV)
E[GSH] True (mV)
R+3%
R−3%
Possible values
roGFP1_R12
E_{GSH}
Expected accuracy (mV)

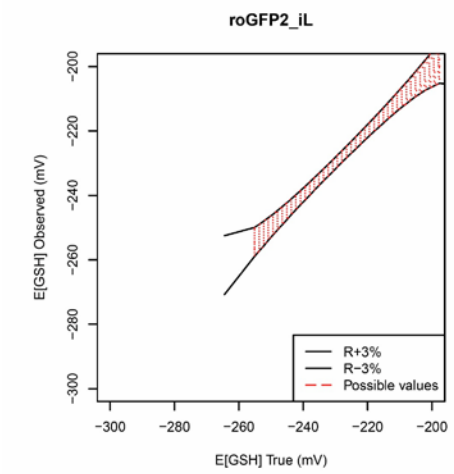
roGFP2_iL
E[GSH] Observed (mV)
E[GSH] True (mV)
R+3%
R−3%
Possible values

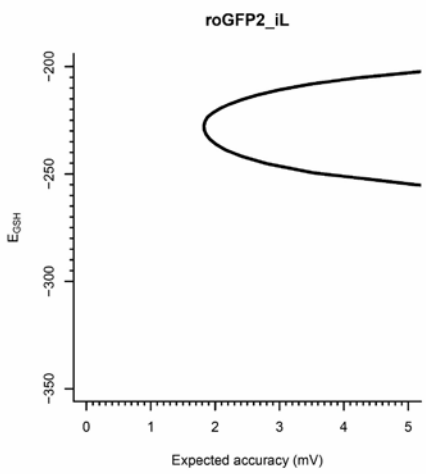
roGFP2_iL
E_{GSH}
Expected accuracy (mV)

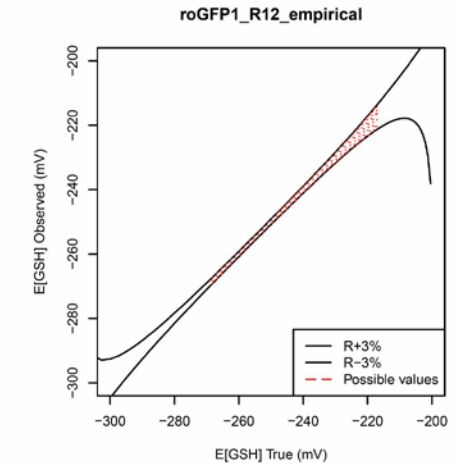
roGFP1_R12_empirical
E[GSH] Observed (mV)
E[GSH] True (mV)
R+3%
R−3%
Possible values

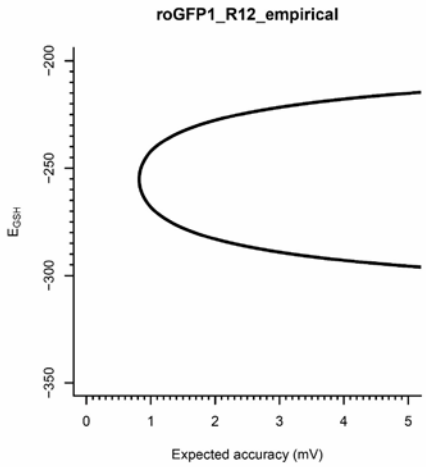
roGFP1_R12_empirical
E_{GSH}
Expected accuracy (mV)

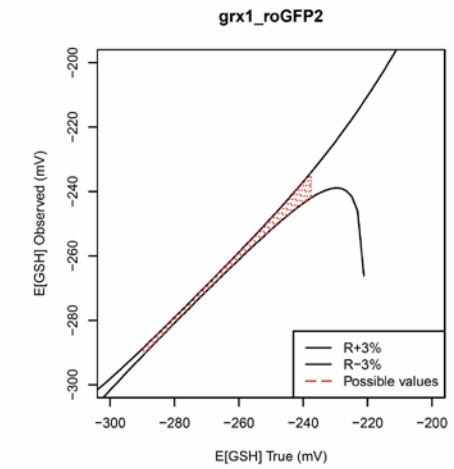
grx1_roGFP2
E[GSH] Observed (mV)
E[GSH] True (mV)
R+3%
R−3%
Possible values

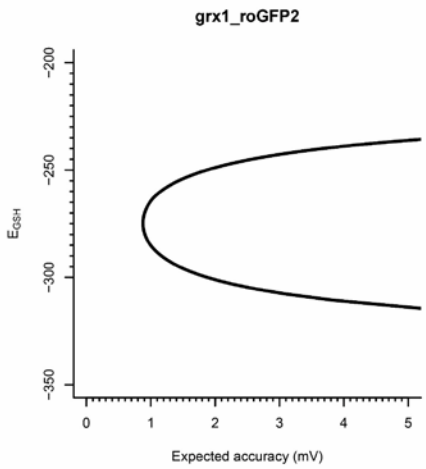
grx1_roGFP2
E_{GSH}
Expected accuracy (mV)

pH Sensors: Spectra

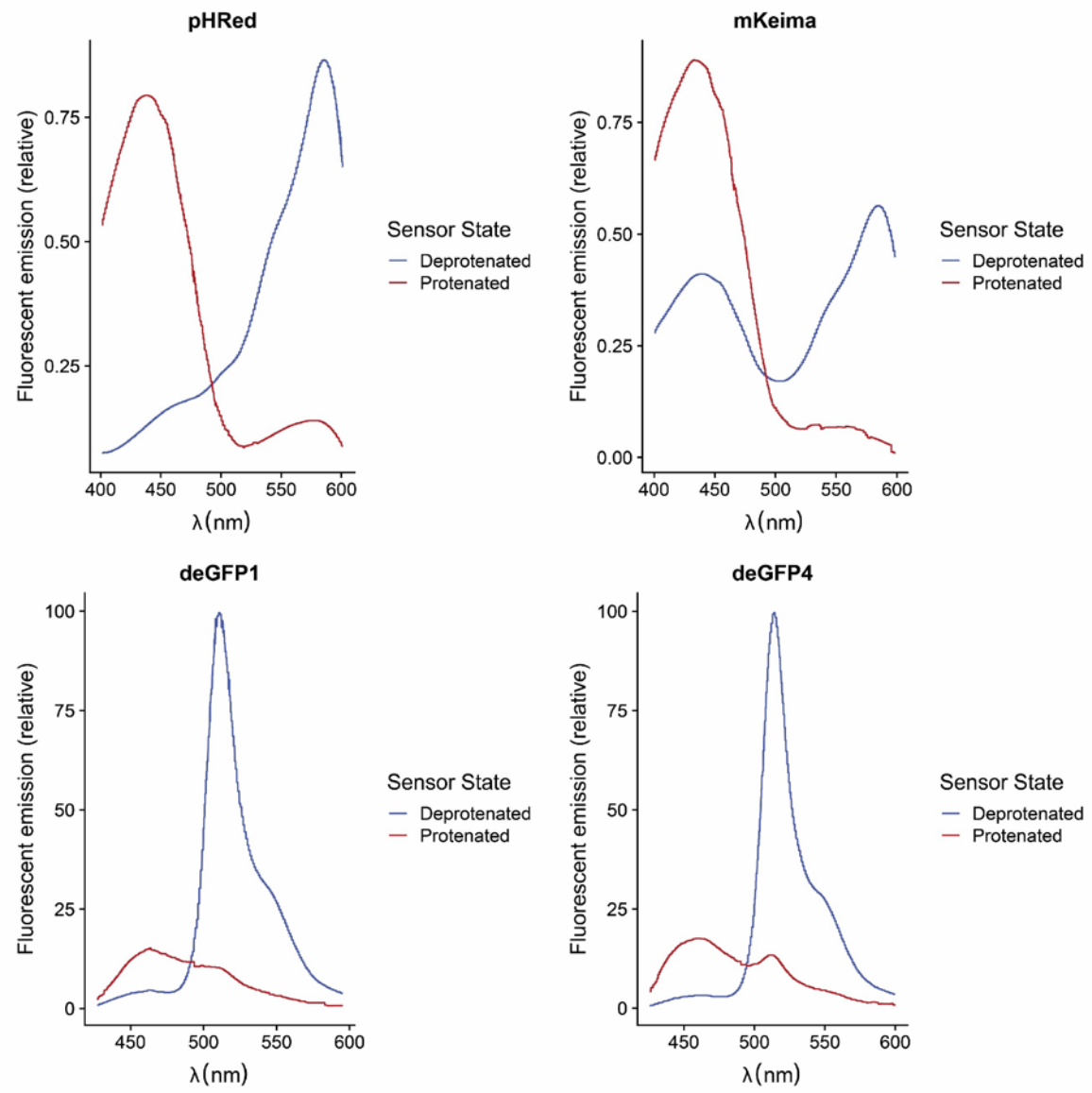

pH Sensors: Observed-actual maps and phase plots